COMBUSTION SYNTHESIS OF FULLERENES AND FULLERENIC NANOSTRUCTURES

P. HEBGEN[*], A. GOEL[*], L.C. RAINEY[†], J.B. VANDER SANDE[†], and J.B. HOWARD[*]

[*]Department of Chemical Engineering
[†]Department of Materials Science and Engineering
Massachusetts Institute of Technology
77 Massachusetts Avenue
Cambridge, Massachusetts 02139

Introduction

Fullerenes were discovered by Kroto *et al.* in 1985 as products of the evaporation of carbon into an inert gas [1]. They consist of closed spherical shells comprised only of carbon atoms. This special structure results in unusual physical and chemical properties with a large potential for applications such as superconductors, sensors, catalyst, optical and electronic devices, polymers, and biological and medical applications. Fullerenes can also be formed in low-pressure fuel-rich flames of certain hydrocarbons [2,3,4], the highest yields being obtained under conditions of substantial soot formation. Other interesting classes of fullerenic or curved-layer carbon that can also be found in fullerene producing systems are nanostructures having tubular, spheroidal, or other shapes and consisting of onion-like or nested closed shells [5,6,7,8] and soot particles having considerable curved-layer content [9,10,11]. More information on the formation of fullerenic carbon in flames under different conditions is needed to understand the formation mechanisms and kinetics and to enable the design of practical systems for large-scale production.

Premixed Flame Studies

Much of the research on fullerene formation in flames has been done with low-pressure, laminar premixed flames of benzene and oxygen with or without inert diluent gas. The setup for these flames is shown schematically in Fig. 1. Part (A) shows the chamber with a microprobe sampling system installed for condensible material collection, while part (B) shows an alternate macroprobe sampling system for the same purpose. The fuel (benzene) and oxygen are fed to the core region of a water-cooled flat flame burner, which is vertically adjustable with a stepper motor. The chamber is evacuated through two vacuum ports located at the bottom of the chamber. A viewport on the side of the chamber allows for visual observation of ignition and flame behavior. The sampling system shown in part (A) consists of a glass wool plug filter inside in an aluminum foil sleeve. The filter is inserted into the flame with a water-cooled quartz microprobe that is connected to a vacuum pump. This probe is vertically adjustable in the flame. The sampling system shown in part (B) consisting of a larger quartz probe with copper collector plates downstream from the probe, permits the collection of larger samples. This probe is also connected to a vacuum pump and the entire unit is

water-cooled. The housing of this probing system is used in place of the chamber top-plate, fixing the location of the macroprobe to a specific height. Both probing systems are designed to minimize effects of the probe on the flame, and both give comparable results.

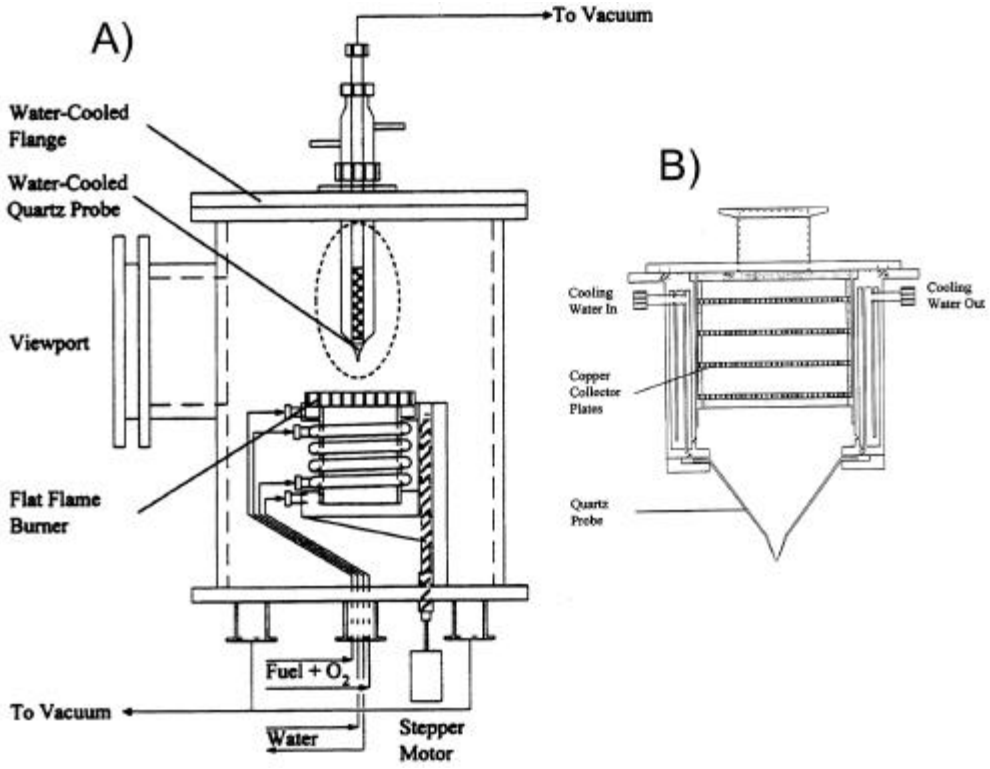

Figure 1. Premixed flame combustion chamber with burner and microprobe sampling system (A) [12] and macroprobe sampling system (B) [4].

In the flames studied in this chamber, the largest yields of fullerenes were observed not under the most heavily sooting conditions, but under conditions where 2-3% of the carbon is converted to soot. With lower fuel/oxygen ratios the amount of fullerenes formed decreases to small amounts near the critical conditions for soot formation. With variations of pressure in the burning chamber, fuel/oxygen ratio, and inert gas dilution, it was possible to produce soots with wide variations in the amount of fullerenes present [3].

Subsequent studies [4] have shown that premixed flames have two distinct fullerene forming regions as can be seen in Fig. 2. The second or later formation region accounts for most of the fullerenes mass produced [4]. Analyses of residence-time resolved soot samples suggest that the formation of amorphous and fullerenic carbon occurs early in the flame, with the fullerenic carbon becoming more curved as a soot particle traverses the length of the flame. Curvature of carbon layers seen in high resolution transmission electron microscopy (HRTEM) images was quantified by measuring the arc length L and diameter D of many layers and computing a curvature parameter defined as $C=L/\pi D$ which ranges from 0 for a planar layer to 1 for a completely closed spherical layer (Fig. 3). The formation of fullerenic nanostructures

under premixed combustion conditions appears to require much longer residence times than the ~70 ms available in the flames [9].

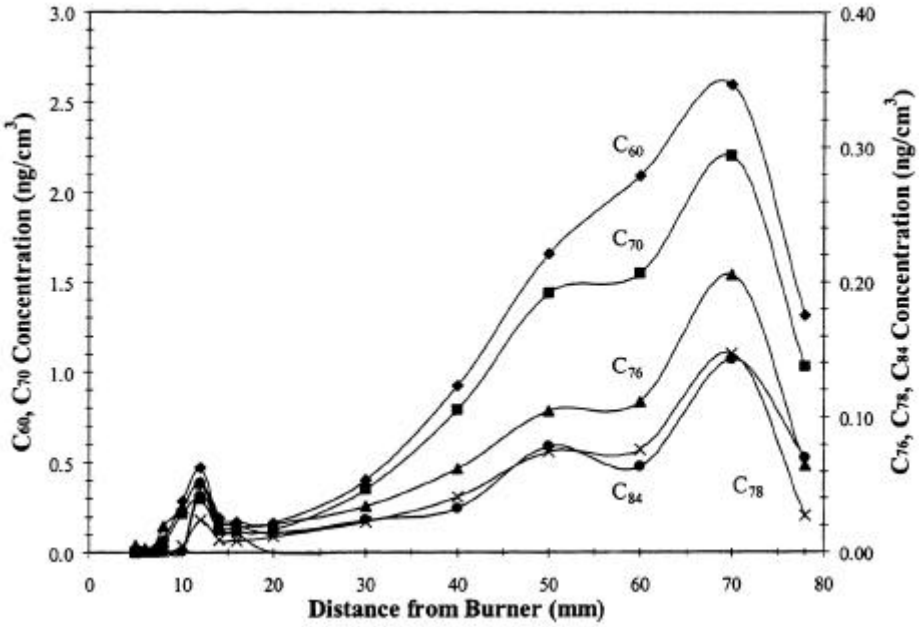

Figure 2. Flame gas concentrations of fullerenes in a premixed benzene/oxygen/argon flame at different axial distances from the burner [4].

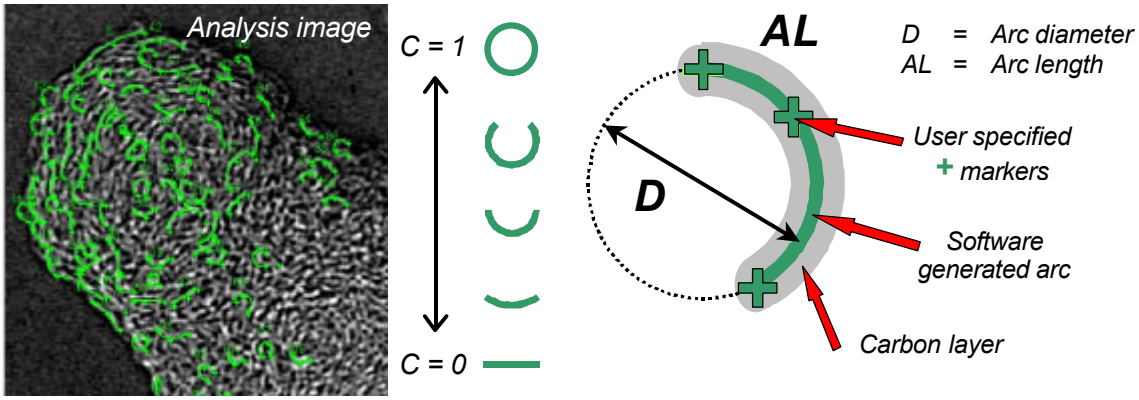

Figure 3. Example HRTEM image with curvature parameter calculation technique.

Diffusion Flame Studies

Fullerenes formation in diffusion flames had received little study until recently although this type of flame, if effective, would offer advantages for practical operation. In recent work [11], fullerenes formation in laminar jet diffusion flames of benzene diluted with argon and burning in oxygen at pressures of 12 to 40 Torr was characterized. The experimental setup used to study these flames is shown in Fig. 4 and described elsewhere [11]. A microprobe sampling system of the type used for premixed flames (Fig. 1A) was also used in studying the diffusion flames (Figure 4). Fuel diluted with argon is injected along the central axis of the combustion chamber through a conical nozzle. Oxygen is fed through a relatively large-diameter porous bronze plate from which it issues with uniform velocity in the annular region

surrounding the fuel stream. The chamber is evacuated through two vacuum ports in the chamber top plate. Both the burner and the probe are vertically adjustable (see two-headed arrows in Fig. 4), allowing a wide range of heights above burner and hence, residence times, to be sampled.

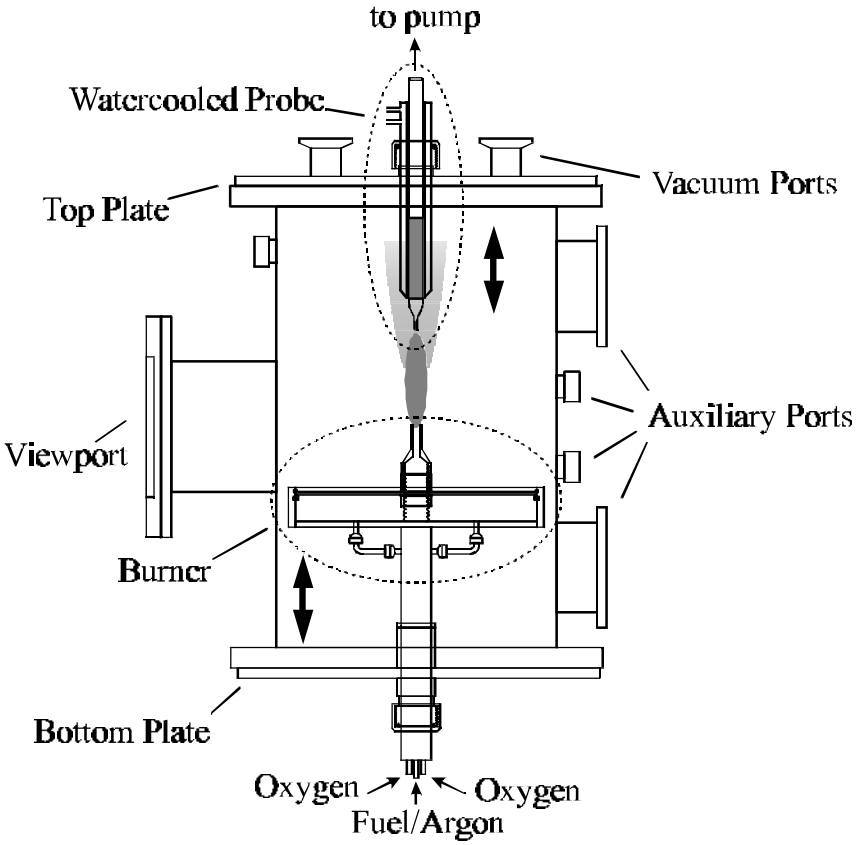

Figure 4. Diffusion flame combustion chamber and microprobe sampling system [11].

The diffusion flames were characterized by measuring the ratios of the mass of fullerenes to the mass of condensable material and to the volume of noncondensable gas. The results show that fullerenes, fullerenic nanostructures, and fullerenic soot can form in diffusion flames with yields and extent of curvature in the soot as large as those seen in premixed flames. The results of the fullerene analysis (Fig. 5) show that every flame exhibited a fullerene maximum and that the concentration of fullerenes generally increased with a decrease in flame length (Fig. 5e), which is indicated by the point of highest fullerene concentration. Also, at given reactor pressure, the ratio of C_{60} to C_{70} decreases with increasing height.

The maximum concentration of fullerenes along the axis of the flame was found just above the stoichiometric surface, near the location of the highest flame temperature and in the region where the concentration of fullerene precursors, which in flames are polycyclic aromatic hydrocarbons (PAH) [13,14,15], is decreasing and fullerenes are beginning to be consumed, both due to oxidation. These consumptions are presumably offset by the increase of fullerene formation rate with increasing temperature and the formation of five-membered rings in the

structure of PAH through oxidation of, followed by CO elimination from, six- membered rings [16]. Surprisingly, the maximum fullerene percentage in the condensables

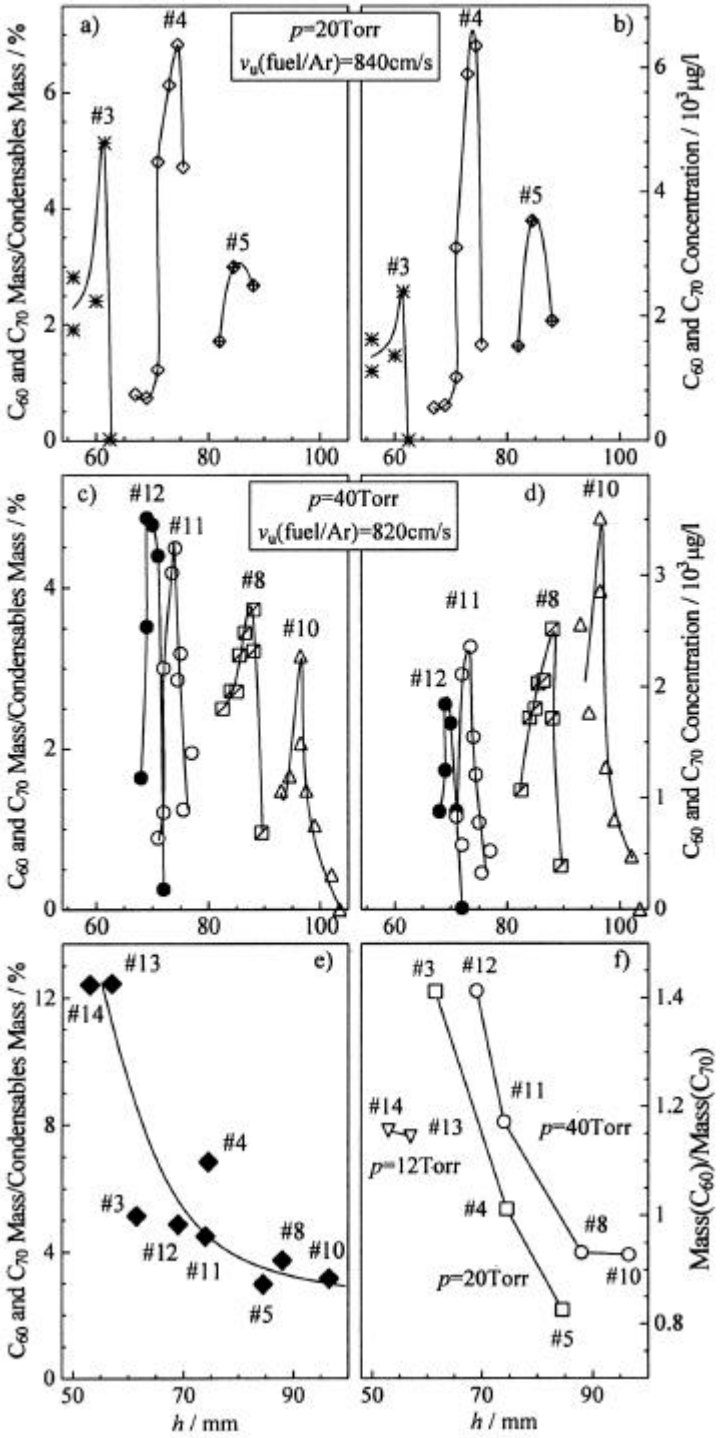

Figure 5. Quantity of fullerenes C_{60} and C_{70} in the condensable material (a, c) and concentration of fullerenes C_{60} and C_{70} in the cold probed gas (b, d) from different heights above the burner in different flames, and maximum amount of fullerenes C_{60} and C_{70} (e)

and mass ratio of C_{60} to C_{70} (f) in the condensable material at the height above the burner corresponding to maximum fullerene concentration in flames, at different pressures (p) [11].

occurs at fuel dilutions as high as 65%. The extent of soot formation decreases with increasing dilution, thereby reducing the radiative heat loss from the flame and increasing temperature until this effect is balanced by the lower production of heat due to less fuel.

The total amount of soot seems to be an important factor for the consumption of fullerenes because, at 40 Torr, the percentage of fullerenes in the condensable material is highest at the highest dilution, but the temperature is lower compared to lower dilutions. At the same time, the concentration of precursors for soot and fullerenes is decreasing. This makes the flame with the lowest total concentration exhibit the highest fullerene percentage. The same effect is seen with decreasing pressure. A lower pressure gives lower soot and fullerene concentrations, but the percentage of fullerenes is still higher. This behavior results in shorter flames yielding a higher percentage of fullerenes in the condensable material.

Discussion

The electron microscope images of soot from fullerene forming flames show a composition that is different from samples collected in higher-pressure flames or conventional combustion systems [9]. However, structures similar to those seen here have also been found in commercially-produced carbon black [17,18]. A representative HRTEM image of condensable material from a fullerene forming diffusion flame (Fig. 6) shows that both fullerenes and curved carbon layers are present. Curvature analysis of this image produces the histograms shown in Fig. 7. Comparison of such histograms obtained for samples from various distances from the burner indicates that fullerene structures, i.e., curved layers, in the soot, as characterized by the curvature parameter, increase up to the location of the fullerene maximum in the gas phase and decline thereafter. This behavior would be expected since the chemical analysis discussed above indicates a similar trend.

An increase in the diameter of layers can indicate either or both of two effects, that layers are actually growing in size and/or that the layers are becoming flatter. Coupling the diameter observations with those from curvature and arc length indicates that the layers are becoming increasingly curved until the fullerene maximum in the gas phase is reached, and then start to become flat, perhaps being incorporated into nanostructures. The diameter data reinforces the conclusions drawn from the curvature data.

The amount of nanotubes and onion-like structures is higher in the diffusion flames than in the premixed flames studied. In the latter case, nanostructures were seen only at long residence times where the oxygen had been depleted. In the diffusion flames, nanostructures appear relatively soon after the stoichiometric flame surface where the maximum temperature occurs and the fullerenes and soot are being oxidized and fullerenes are being incorporated into the soot. At longer residence times, the closed structures in the soot disappear, while at the same time, we find nested structures and, separated from the soot, nanostructures. Consequently, the time-scale for nanostructure formation in diffusion flames must be shorter than that for premixed combustion. The HRTEM analysis of the soot material indicates that the

nanostructures are formed directly from curved structures in the soot. An HRTEM image of fullerenic nanostructures from collected diffusion flame material is shown in Fig. 8. In addition to fullerenic nanostructures, larger fullerene molecules have also been observed here, as in prior combustion studies [4,19,20].

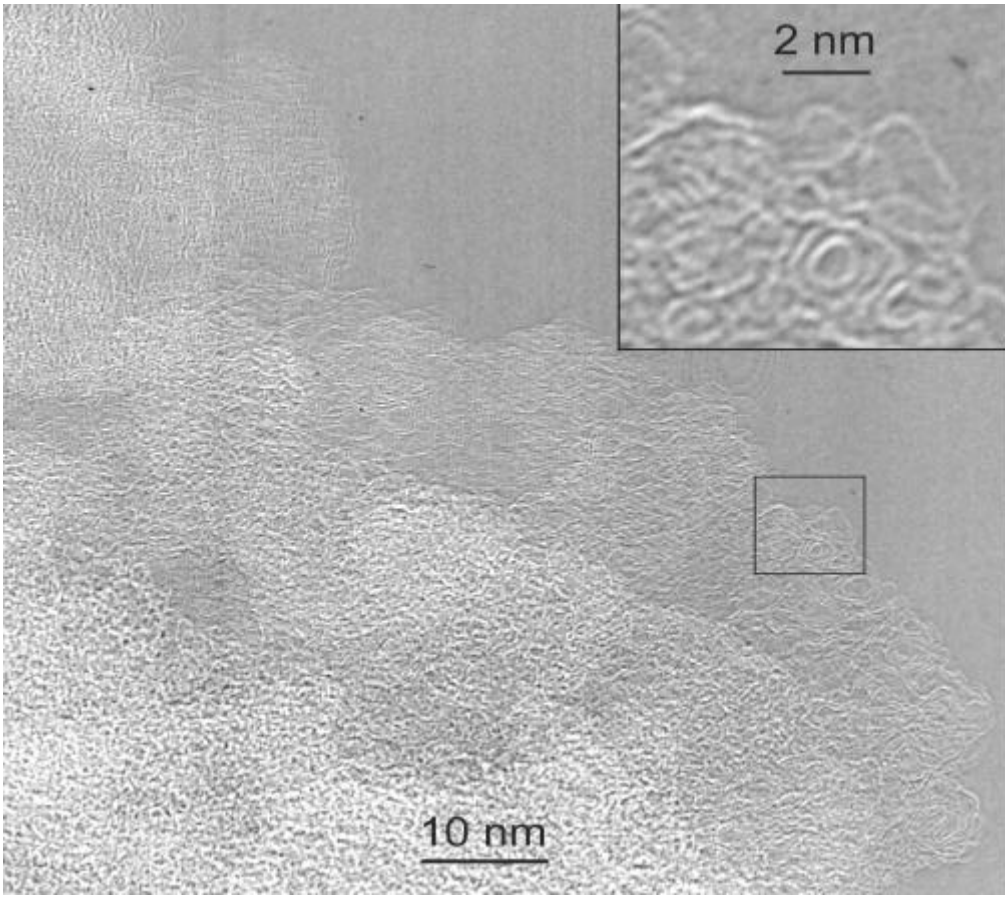

Figure 6. HRTEM image of condensable material (pressure = 40 Torr, argon dilution = 85.3%, height above burner = 75 mm) [11].

The mechanism of fullerenes formation in flames is still not clear but studies suggest that they are formed by reactions generating PAH which can form fullerenes as well as soot particles. Mechanisms involving carbon clusters as chains and rings have been identified in carbon arc vaporization production methods [21-24]. However, these mechanisms are not suitable for combustion synthesis because the concentration of these clusters is too small [20]. Consequently, several other mechanisms for fullerene formation in flames have been proposed.

Pope *et al.* [25] suggest that fullerenes may be formed in combustion through the stepwise addition of acetylene to a single PAH molecule, through the reactive coagulation of two PAH molecules, or through hydrogen elimination followed by ring closing. Pope *et al.* also indicate the intramolecular rearrangements may play a role in fullerene formation.

As mentioned previously, the precursors of fullerenes and other fullerenic material may be PAH with curvature arising from embedded five-membered rings. Baum *et al.* [20] suggest

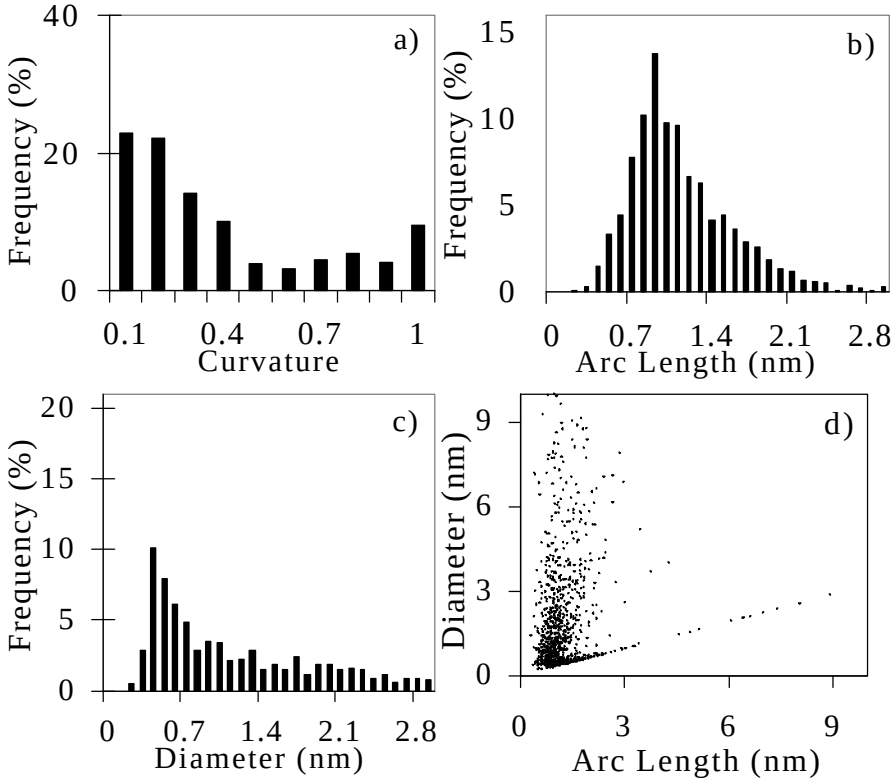

Figure 7. Normalized histograms of curvature (a), arc length (b), and diameter (c) and arc length vs. diameter scatterplot (d) of condensable material (pressure = 40 Torr, argon dilution = 85.3%, height above burner = 75 mm) [11].

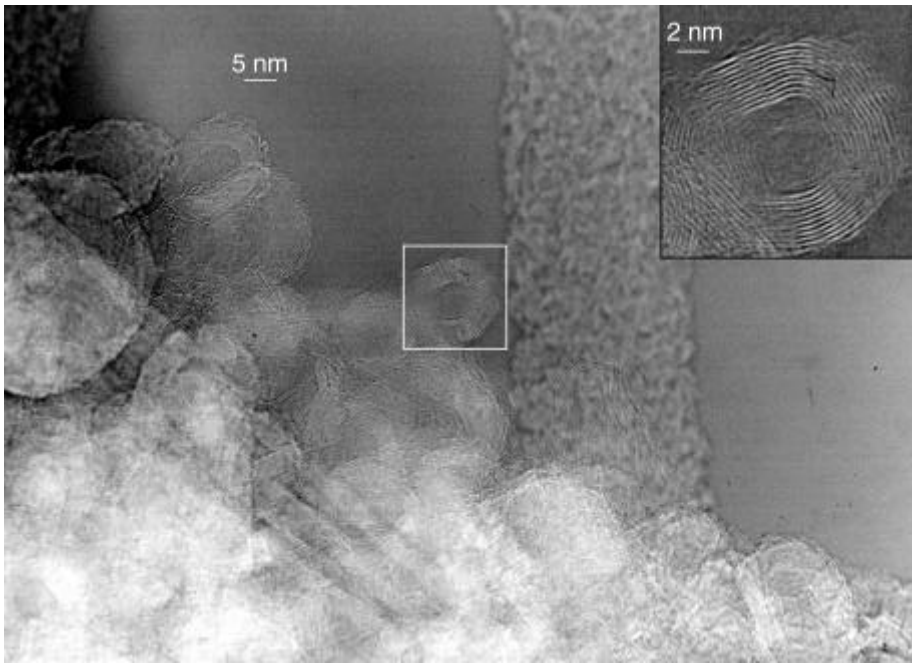

Figure 8. HRTEM image of fullerenic nanostructures in collected condensable material (pressure = 12 Torr, argon dilution = 65.0%) [11].

that this is a plausible mechanism for fullerene formation as opposed to a direct route from polyynes to fullerenes. Baum *et al.* argue that the large rate of positive fullerene ion formation is a strong argument that PAH and their ions are precursors of fullerenes and fullerenic ions, respectively.

Also, as discussed above, gas-phase as well as condensed-phase reactions may be involved. For gas-phase synthesis, Baum *et al.* [20] present a zippering mechanism. In this mechanism, two large PAH molecules that are nearly planar align so as to zip their edges together through hydrogen elimination. This mechanism also involves the simultaneous internal rearrangement of the PAH to form the five-membered rings that are characteristic of fullerenes. Alternatively, the five-membered rings may already be present as it is possible that two PAH with bowl-like structures participate in the zippering mechanism [25]. Baum *et al.* [20] also suggest a condensed-phase mechanism in which young soot particles act as reactors for fullerenes. According to their picture, surface growth of these particles and arched subunits within, along with internal rearrangement of the soot can lead to closed shells that can then evaporate from the rest of the particle.

There are also mechanistic implications in the data presented above. It is thought that oxidation reactions are responsible both for fullerene and precursor consumption but that the highest concentrations of fullerenes occur where the precursor concentration is already decreasing [11]. This suggests that fullerene formation is also dependent on temperature as this location coincided with the highest observed flame temperature. Additionally, the presence of a fullerene maximum with respect to dilution indicates that fullerene formation is defined by the competing effects of reduced radiative heat loss and reduced heat production. Observations of

longer residence times in the flames also suggest that nanostructures are formed much later than fullerenes and that fullerenes may be incorporated into the soot.

Finally, it has also been shown that pressure, temperature, fuel type, and residence time all affect the relative amounts of curved and planar PAH formed, the yield of fullerene molecules, and the relative amounts of fullerenic and graphitic carbon in the particles. In addition to experiments on pressure and temperature effects in benzene flames [4,9,11], studies have been done using fuels such as naphthalene [26], butadiene [26], toluene [27], and organics with halogen additives [28]. Of pure fuels, it was found that benzene produces the greatest amounts of fullerenes [3,11,26,27], but production could be enhanced with a chlorine additive [28]. It also appears that lower pressures and higher temperatures result in higher fullerene concentrations [11] but operating conditions have not been optimized.

Acknowledgements

We are grateful to David Kronholm for development of image analysis software, to Murray Height for preparation of Figure 3, and to William Grieco for premixed flame data. Different parts of the work described here were supported by the National Aeronautics and Space Administration (Grant No. NAG3-1879) and the Division of Materials Sciences (Grant No. DE-FG02-85ER 45179) and the Division of Chemical Sciences (Grant No. DE-FG02-84ER 13282), Office of Basic Energy Sciences, Office of Energy Research, U.S. Department of Energy.

References

[1] Kroto, H.W., Heath, J.R., O'Brien, S.C., Curl, R.E., Smalley, R.E., *Nature* **318**: 162 (1985).
[2] Howard, J.B., McKinnon, J.T., Makarovsky, Y., and Lafleur, A.L., and Johnson, M.E., *Nature* **352**: 139 (1991).
[3] Howard, J.B., Lafleur, A.L., Makarovsky, Y., Mitra, S., Pope, C.J., and Yadav, T.K. *Carbon* **30**: 1183 (1992).
[4] Grieco, W.J., Lafleur, A.L., Swallow, K.C., Richter, H., Taghizadeh, K., and Howard, J.B., *Proc. Combust. Inst.* 27: 1669 (1998).
[5] Iijima, S., *Nature* **354**: 56 (1991).
[6] Ugarte, D., *Carbon* **33**: 989 (1995).
[7] Howard, J.B., Chowdhury, K.D., and Vander Sande, J.B., *Nature* **370**: 603 (1994).
[8] Chowdhury, K.D., Howard, J.B., and Vander Sande, J.B., *J. Mater. Res.* **11**: 341 (1996).
[9] Grieco, W.J., Howard, J.B., Rainey, L.C., Vander Sande, J.B., *Carbon* **38**: 597 (2000).
[10] Werner, H., Herein, D., Blöcker, J., Henschke, B., Tegtmeyer, U., Schedelniedrig, T., Keil, M., Bradshaw, A.M., Schlogl, R. *Chem. Phys. Lett.* **194**: 62 (1992).
[11] Hebgen, P., Goel, A., Howard, J.B., Rainey, L.C., and Vander Sande, J.B., *Proc. Combust. Inst.* 28 (2000). [in press]
[12] McKinnon, J.T., Ph.D. Thesis, Massachusetts Institute of Technology (1989).
[13] Ahrens, J., Bachmann, M., Baum, T., Griesheimer, J. Kovacs, R., Weilmünster, P., and Homann, K.-H., *Int. J. Mass Spectrom. Ion Processes* **138**: 133 (1994).
[14] Pope, C. J., Marr, J. A., and Howard, J. B., *J. Phys. Chem.* **97**: 11001 (1993).
[15] Lafleur, A.L., Howard, J.B., Marr, J.A., and Yadav, T., *J. Phys. Chem.* **97**: 13539 (1993).

[16] Bittner, J.D., and Howard, J.B., *Proc. Combust. Inst.* 18: 1105 (1981).
[17] Donnet, J.B., *Rubber Chem. Technol.* **71**: 323 (1998).
[18] Donnet, J.B., Wang, T.K., Wang, C.C., Monthioux, M., Johnson, M.P., Norman, D.T., Wansborough, R.W., and Bertrand, P., *KGK Kautschuk Gummi Kunststoffe* Hüthig GmbH, Hiedelberg, 1999, p. 340.
[19] Richter, R., LaBrocca, A.J., Grieco, W.J., Taghizadeh, K., Lafleur, A.L., and Howard, J.B., *J. Phys. Chem.* **101**: 1556 (1997).
[20] Baum, T., Löffler, S., Löffler, P., Weilmünster, P., and Homann, K.-H. *Ber. Bunsenges. Phys. Chem.* **96**: 841 (1992).
[21] Krestinin, A.V., and Moravsky, A.P. *Chem. Phys. Lett.* **268**: 479 (1998).
[22] Helden, G.V., Hsu, M.-T., Gotts, N., and Bowers, M.T. *J. Phys. Chem.* **97**: 8182 (1993).
[23] Hunter, J.M., Fye, J.L., Roskamp, M.F., and Jarrold, M.F. *J. Phys. Chem.* **98**: 1810 (1994).
[24] Strout, D.L., and Scuseria, G.E. *J. Phys. Chem.* **100**: 6492 (1996).
[25] Pope, C.J., Marr, J.A., Howard, J.B., *J. Phys. Chem.* **97**:11001 (1993).
[26] Ahrens, J., Bachmann, M., Baum, T., Greisheimer, J., Kovacs, R., Weilmünster, P., and Homann, K.-H. *Int. J. Mass Spec. Ion Proc.* **138**: 133 (1994).
[27] Richter, H., Fonseca, A., Thiry, P.A., Gilles, J.-M., Nagy, J.B., and Lucas, A.A. *MRS, 1994 Fall Meeting*, (1994).
[28] Richter, H., de Hoffman, E., Doome, R., Fonseca, A., Gilles, J.-M., Nagy, J.B., Thiry, P.A., Vandooren, J., and Van Tiggelen, P.J. *Carbon* **34**: 797 (1996).